ICAS-88-2.5.1

NEW GUIDE FOR ACCURATE NAVIER-STOKES SOLUTION OF TWO-DIMENSIONAL EXTERNAL COMPRESSION INLET WITH BLEED*

C. K. Forester and E. Tjonneland
Boeing Advanced Systems
Seattle, Washington

Abstract

Conventional means of insuring accurate Navier-Stokes analysis are not reliable, nor very specific. A new approach is being developed to streamline and simplify this process. Direct measures of solution error sources are being explored. The artificial diffusion ratio (ADR), is a candidate error monitor because grid-related errors are caused and controlled by artificial diffusion. Residual contamination of the dependent variables and their derived quantities is also manifest as a diffusive type of error and these errors are registered by ADR.

An example of using ADR to guide the Navier-Stokes analysis of a supersonic external compression inlet with bleed flow is provided. The inlet throat region flow is mixed supersonic and subsonic flow with large viscous interactions. These interactions are due to shocks generated by special geometric features of the configuration. Shock/shear-layer/expansion-fan interactions have small length scales relative to the inlet dimensions. The utility of ADR for guiding grid selection to generate an accurate solution is illustrated. Further work is recommended to develop the technique for use in analysis comparisons with benchmark experiments or in certifying final configuration selection in aircraft development projects. Further work is recommended to develop the use of ADR error monitors for general use in grid and in smoothing level selection.

List of Symbols

ADR	artificial diffusion ratio
ADRF	u - momentum ADR
ADRG	v - momentum ADR
ADRH	energy ADR
ADRR	mass density ADR
C	a constant
F	u-momentum flux
G	v momentum flux
H	total energy
m	time step index
P	pressure
R	density
t	time coordinate
u	x-direction velocity
x	x-direction coordinate
y	y-direction coordinate
ν	diffusion coefficient

Subscripts

a	artificial diffusion coefficient
FL	Courant, Friedrichs, Lewy condition
i	integer grid index in x-coordinate direction
L	linear
M	MacCormack
S	smoothing
t	total or stagnation condition
∞	freestream condition

I. Introduction

The purpose of this paper is to introduce a new concept to guide the selection of the grid for applying Navier-Stokes analysis to flow fields of engineering interest. This new guide is designed to indicate grid resolution problems. It is based upon using data already available in the numerical process of Navier-Stokes analysis tools and can readily be formatted for graphical output. An inlet design test problem was chosen for demonstrating the concept.

Future tactical aircraft with stringent maneuverability requirements will likely require external compression inlets. The viability of this concept in the Mach 2.2 to 2.5 range is dependent upon special tailoring of the throat bleed flow and slot geometry for stable engine-face flow delivery with minimum losses. The spillage drag of this inlet concept is critically dependent upon the design of the bleed flow system. Engine face flow quality is a by-product of the ramp/cowl/bleed system design. Minimum spillage for shock stability and low engine face flow distortion promote propulsion efficiency and enhanced control characteristics.

Analysis tools are being developed to improve the efficiency of the design of external compression inlets. For three-dimensional analysis, Paynter and Chen,[1] and Anderson[2] have made considerable progress. 3-D analysis will aid the design of test configurations and aid in certifying the choice of the full-scale configuration. Analysis will also enhance the degree of integration of the propulsion system with flight controls, airplane aerodynamics, and structural requirements. The proper integration of these elements is the key to high performance in the aircraft.

* This research was sponsored by the Air Force Office of Scientific Research (AFSC), under Contract F49620-85C-0126. The United States Government is authorized to reproduce and distribute reprints for governmental purposes notwithstanding any copyright notice hereon.

II. Discussion of Error Sources

The interaction of all the relevant flow regimes for the present inlet analysis require a Navier-Stokes flow solution. These equations and their boundary conditions are precise, exact and continuous. The process of numerically simulating these equations is not precise, exact or continuous. Numerical solutions of these field equations involve solving equations which have additional properties that are not contained by or related to the continuous equations. These additional properties are caused by the choice of the algebraic structure used to model the continuous equations.

There are three categories of these additional properties which create spurious, phase and diffusive behavior in the solutions. Examples of spurious behavior arise from mass sources and sinks; or negative density or temperature; decay of entropy or increases in available total pressure; or simply the oscillation of some property in a region where it should be a smooth function. Phase shifts result from dispersive error properties of the algebraic structure. Diffusive behavior is manifested by poor acuity of steep gradients or by damped peak amplitudes of dependent variables or their derived quantities. When special conditions (discussed later in this paper) are satisfied, adequate control of numerical accuracy is achieved. Satisfying these conditions results in a well-behaved relation between the field equations and the computational analysis model. These conditions may be satisfied by observing a function that defines a multi-dimensional mapping of errors to be minimized, called the error-space map. This error mapping function contains the influence properties of truncation, residual and round-off error.

Principle factors influencing the behavior of the error mapping function include the choice of the artificial viscosity level, the grid shape, the grid density distribution, the residual level and the computer dependent factor of round-off error. Each of these factors directly contribute to the numerical error in the computed solution.

In the present study, error monitors are sought to direct the analysis process for achieving "good" grids - those grids giving solutions suitable for engineering application. To focus the discussion on diffusive error sources, the two categories of error sources (residual error and truncation error) are discussed under the umbrella of artificial diffusion .

The use of time relaxation to asymptotically approach steady state solutions produces an error called the residual, the remnant in the time-like terms that is non-zero. From arbitrary initial conditions, the residual spectrum has mostly high frequency content, the magnitude of residuals change dramatically cell-to-cell in certain regions of the flow field. This feature of the initial conditions produces shock-like jumps in the dependent variables. These jumps create problems in getting the Navier-Stokes codes to converge. The role of artificial diffusion is critical in dissipating these perturbations and driving them from the analysis domain. The convergence to steady state (the reduction of residual error toward machine zero) depends upon the artificial dissipation functions working properly. Therefore the primary focus of the discussion of error sources is on artificial diffusion.

Every form of numerical approximation of the Navier-Stokes equations, whether finite difference, finite volume or finite element, possesses artificial diffusion. It is added through auxiliary explicit or implicit smoothing operators for symmetric discretization operators. It is included implicitly in asymmetric discretization operators, whether they are explicit or implicit upwind expressions. Artificial diffusion in upwind asymmetric schemes can be quantified by computing all convective fluxes by symmetric difference schemes of comparable order of accuracy. The smoothing flux is simply the difference between the fluxes of the comparably accurate symmetric and asymmetric schemes. This conclusion is based upon generalizing MacCormack's[4] error analysis using Taylor expansions.

There is a difference in the magnitude of smoothing requirements between linear and nonlinear regions of the flow analysis domain. For example, regions of the flow featuring shocks (nonlinear) require enormous smoothing levels. Since shock waves abound in large numbers (as discussed previously) during the early stages of the convergence process, the initial smoothing requirements are for high levels of smoothing in most of the flow analysis domain.

As the converged solution is approached, the smoothing levels must be low except in shock regions and poorly resolved flow regions that behave like discontinuities. Inadequate grid resolution in some regions of the analysis domain lead to unresolved flow regions. These regions impose demands upon the smoothing operator to keep the computations stable causing higher than desirable smoothing levels. Complexity is inherent in the widely varying demands for smoothing during the convergence process. The smoothing operator developed by MacCormack[4] copes with the early requirements for massive global damping while providing highly tailored damping for optimum grid utilization.

Artificial diffusion is specifically added to smooth, stabilize and enhance the convergence characteristics of centered difference operators for Navier-Stokes solution algorithms such as the MacCormack finite volume predictor-corrector scheme. This is done by constructing a smoothing flux. It is added explicitly to the raw flux in the predictor-corrector cycles. The impact on the solution accuracy of this smoothing operator, relative to grid and residual effects, has been obscure.

III. Discussion of the Error Monitors

A new approach is being developed to streamline and simplify the process of selecting an analysis grid. Direct measures of solution error sources are being explored, these include measures of total pressure error and the artificial diffusion defined in the following paragraphs. Cross-correlation of these, plus other error measures, such as conservation error in local and integral form, have been examined to single out the best guides for selecting grid and smoothing levels. The artificial diffusion ratio (ADR) will be shown to be an excellent candidate for an error monitor.

Instead of looking at results which include smoothing effects, we propose looking at the artificial smoothing itself and its role in compromising the accuracy of the numerical solutions. This way, the main cause of the loss in accuracy is monitored and utilized to select grid densities that ensure accuracy of the analysis process. It will be shown that the artificial diffusion will be large on inadequate or coarse grid solutions where flow gradients are large. This information is used to adjust grid density until the artificial diffusion is minimized and an accurate solution is obtained.

One mechanism for obtaining a measure of the artificial diffusion involves constructing the ratio of the smoothing flux and the total flux through computational cell faces. This ratio is called the Artificial Diffusion Ratio (ADR). By definition, this ratio should be insignificant everywhere in the flow analysis domain except in shock waves. Viscous stagnation regions, viscous bifurcation points, viscous saddle points, viscous shear layers, smooth rotational inviscid regions, smooth irrotational inviscid regions and freestream uniform flow regions must have low levels of artificial smoothing or small values of ADR relative to the peak values of ADR. Coarse grid simulations lead to the treatment of each of these smooth regions as singularities. For example, free shear layers with too sparse a grid become contact surfaces. Bifurcation, saddle and stagnation regions become singular points, lines or surfaces. ADR will register high values in such regions, where indeed ADR would have small values if the grid resolution were correct.

ADR is generated for each dependent variable of the compressible time-averaged Navier-Stokes equations. The dependent variable are two components of momentum (F,G), total energy (H) and mass density (R). These dependent variables result in four artificial diffusion ratios - ADRF, ADRG, ADRH and ADRR, respectively. A composite of these individual error monitors may be constructed by averaging the individual error monitors. All error measures are normalized to achieve peak values not exceeding unity.

To make the discussion clear, the error measures that have been explored are defined mathematically in the next section. Finite difference expressions are used for this purpose. They are derived directly from but not limited to the MacCormack two-step algorithm. To save space only the Burger's equation is reviewed rather than presenting the full momentum, energy and mass conservation equations. Special note should be observed that the error monitors are separate, post-processor elements from the MacCormack algorithm and can be used with any numerical algorithm for the Navier-Stokes equations.

A. Mathematical Definition

The concept of error analysis for numerical approximations of the Navier-Stokes equations can be illustrated using a model equation called the Burger's equation. The Burger's equation in nonlinear form may be written as follows:

$$\frac{\partial u}{\partial t} + \frac{\partial F}{\partial x} = 0$$

where,

$$F = \frac{u^2}{2} - \nu_i \frac{\partial u}{\partial x}$$

Writing a first order forward difference expression for the first derivative of u yields

$$F_i = \frac{(u_i)^2}{2} - \nu_i \frac{(-u_i + u_{i+1})}{\Delta x}$$

To ensure solution stability the viscosity is augmented by adding artificial

viscosity, ν_a, computed as follows:

$$\nu_a = \min \left[0.25, \nu_M\right]$$

The MacCormack viscosity, ν_M, is given by

$$\nu_M = \max \left[C_{FL} \; C_M \frac{\left| u_{i+1} - 2u_i + u_{i-1} \right|}{(u_{i+1} + 2u_i + u_{i-1})}, \; \nu_L\right]$$

and,

$$\nu_L = \max \left[C_L \frac{m-n}{n}, \; 0 \right]$$

The constants C_L and C_M are input values used to scale the magnitude of the added artificial viscosity. The constant m is a specific value that determines the number of time steps required to ramp the linear artificial viscosity, ν_L down to zero.

The resulting artificial viscosity will have an initially high value to aid initializing the solution. After the mth time step (normally set to approximately 200) the artificial viscosity will have a very small magnitude, except in regions of velocity oscillations. For these regions the truncation error is producing erroneous results.

The purpose of the error monitor is to identify such regions. Therefore a smoothing flux is defined as

$$F_S = \nu_a \frac{\partial u}{\partial x}$$

and the artificial diffusion ratio, ADR, is defined as

$$ADR = \frac{|F_{s,i}|}{|F_i| + |F_{s,i}|}$$

The absolute values are taken to insure that ADR is always positive. Therefore,

$$ADR = \frac{\left|\nu_{a,i} \dfrac{(-u_i + u_{i+1})}{\Delta x}\right|}{\left|\dfrac{(u_i)^2}{2} - \nu_i \dfrac{(-u_i + u_{i+1})}{\Delta x}\right| + \left|\nu_{a,i} - \dfrac{(-u_i + u_{i+1})}{\Delta x}\right|}$$

The ADR may be defined similarly for the continuity equation, the two components of the momentum equation, and for the energy equation. These quantities are called ADRR, ADRF, ADRG, and ADRH, respectively.

B. Minimizing Errors

The equations of the previous section constitute a vector of unknowns whose range is determined by the total number of grid points. The number of grid points is chosen rather arbitrarily until data is available on the truncation error spectrum. Once this data exists, a systematic process for minimizing the error is defined as follows.

It should be noted that Burger's equation has analytical solutions for certain initial and boundary conditions. These solutions may be used to exactly define the basis for assessing the truncation and residual errors. It is desirable to show how the errors are minimized by use of the analytical solutions. To save space, these results are summarized without supporting detail.

The residual error level is chosen so that the truncation error estimate is reliable, the residual error must be less than the magnitude of the most important truncation error which must be minimized. This guiding truncation error must be used to direct the process for mesh refinement for all regions in the analysis domain (except discontinuities where the truncation error is arbitrarily large) The grid distribution in physical space is chosen to make the guiding truncation error uniform over the physical space. Once the grid distribution is arrived at, the accuracy of the numerical approximation can be increased arbitrarily by increasing the number of grid points. With these definitions in mind, the error monitors described above can be evaluated exactly. If this is done, a correlation emerges between the truncation error and ADR. It is this correlation which is critical to the viability of ADR as a useful error monitor.

IV Test Problem

To test the error monitors, a Navier-Stokes analysis problem is necessary with manageable application costs to achieve arbitrarily high accuracy. It must also be a problem for which high quality test data exist so that meaningful comparisons can be made. The inlet/aperture flowfield test problem presented is qualified on both accounts.

A. Geometry and Flow

Illustrated in Figure 1 is a supersonic inlet throat region geometry and the flow physics associated with an external compression inlet with throat bleed flow. The inlet/aperture approach flow, parallel to the centerbody ramp, is at the throat design Mach number of 1.28. The bulk of the flow in the streamtube spanning the gap between the cowl lip and ramp crown is captured by the inlet.

Some spillage flow may occur at the cowl lip, depending on the engine face flow and the bleed slot flow requirements. The cowl position establishes a cowl shock wave which impinges on the ramp boundary layer downstream, but near the crown of the ramp. The ramp shock-wave/boundary-layer interaction is stabilized in this position by bleeding flow into a slot opening in the ramp. This slot is downstream of the crown of the ramp. The crown of the ramp generates an expansion fan which locally accelerates the flow to a higher Mach number ($\simeq$1.7) before the flow arrives at the slot opening. These flow physics generate a complex interaction of the cowl shock wave, ramp boundary layer and the ramp crown expansion fan. Interaction produces a free shear layer across the slot opening which has strong viscous generated transverse velocity gradients and strong local inviscid transverse velocity gradients in the supersonic tongue. Further, this flow region is strongly influenced by the slot geometry and amount of bleed flow. These influences reside primarily in the longitudinal direction. The principal agent for this longitudinal contortion of the flow is dictated by the downstream lip of the slot opening. This lip produces a strong shock wave ($M_1 \simeq 1.7$) in the slot region. It is a stronger shock than the cowl shock and much more local with high curvature. This curvature adjusts the flowfield in the neighborhood of the slot opening so that the resultant flow downstream of the slot opening is subsonic to match the static pressure of the remaining flow captured by the inlet.

The slot shock and the shear layer interaction are sensitive to the supersonic flow originating from the ramp crown. Incomplete Prandtl-Meyer expansion in the numerical solution dramatically reduces slot shock strength, and in the extreme case, produces no slot lip shock. Over-expansion in the solution leads to misdirecting the slot free-shear layer to the slot lip. Either of these mismatches lead to incorrect slot pressure, either too high or too low respectively. In turn, the slot flow entrance separation point is affected dramatically by the pressure in the bleed flow opening. The nature of the recirculation flow field impinging upon the bleed entrance free shear layer is subject to change according to the separation point which induces feedback upon the bleed entrance pressure.

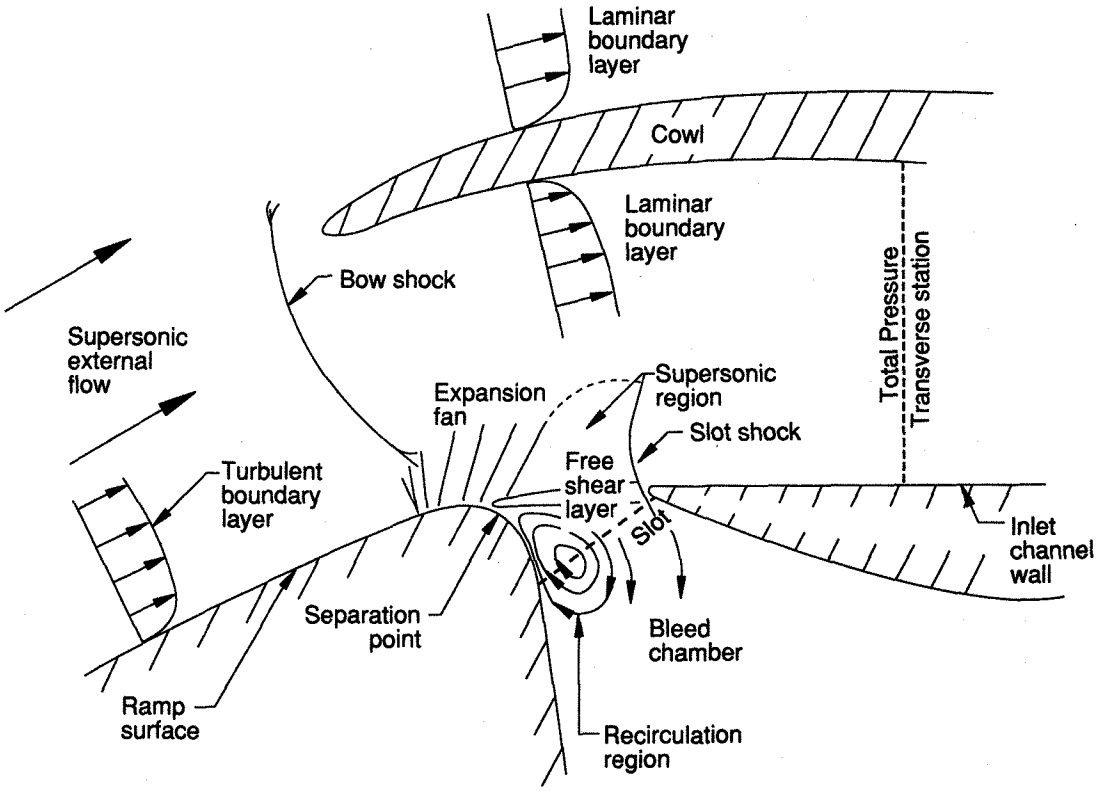

Figure 1. Inlet-Aperture Flow Field Features

Turbulence in the bleed entrance and in the bleed cavity affect the flow pressure at the bleed entrance. The ratio of the length of the bleed flow opening and the thickness of the free shear layer, plus the pressure gradient in the free shear layer, influence the structure of the turbulence in the bleed cavity and in the free shear layer. Favorable pressure gradients accelerate the wall boundary layer at the crown of the ramp. Mixing zone intensity is excited by adverse pressure gradients which prevail between the bleed cavity and the supersonic flow regions. Feedback between the turbulence and the pressure field can cause unsteadiness or instability of the flow at the bleed slot entrance. The intensity of the mixing can be damped or amplified by the unsteadiness. The mixing process may include at least five types of flow:

1) nearly laminar flow of the wall boundary layer at the ramp crown and downstream of the separation point,

2) transition to steady flow mixing between the fully developed supersonic flow and the bleed cavity flow field,

3) possible vigorous flow mixing between the established bleed flow opening free shear layer and the bleed cavity flow field,

4) possible resonance phenomena of the free shear layer and the bleed cavity flow field, and

5) fully developed mixing in boundary and free shear layers.

The occurrence of these types of flow phenomena depends upon flow transition parameters. Model scale inlets and full scale inlets have transition parameters of very different magnitude. For the model scale inlet, examined in the present study, only flow types 1, 2 and 5 have been identified. Numerical experiments indicate that only type 5 flow dominates the wall boundary layers and free shear layers.

B. Computational Approach

The computational approach in the present study is an extension of the work of Peery and Forester[3]. It uses a conservation-based body-fitted adaptive grid model of the thin-shear-layer formulation of the compressible, Reynolds-averaged, Navier-Stokes equations together with mass and energy conservation equations.

Control of the residual errors is achieved, by an artificial time relaxation approach with a constant CFL criteria. Steady state is achieved by asymptotic time relaxation. Truncation errors are reduced through the use of solutions on varying grid densities and varying grid distributions. The formulation of (a) the governing thin-shear-layer equations, (b) the finite volume explicit predictor-corrector finite difference algorithm, (c) the boundary conditions, (d) the two-layer algebraic turbulence model with its associated wall functions, and (e) the mesh generator and the adaptive mesh mover are detailed by Campbell and Forester[7] and the associated references. The procedure for design application of this code is given by Campbell, Syberg and Forester.[8] Smoothing has been applied to the coefficients of the smoothing algorithm to obtain consistent convergence. Without this feature, limit cycles of the smoothing coefficient would occasionally prevent convergence to steady state. Steady state convergence is now reliable.

The computer program allows three coupled computational regions. In the present study, computational region one (see Figure 2) is assigned to the slot cavity flow field, computational region two is assigned to the ramp/cowl/engine face flow region, and computational region three is assigned to the above-the-cowl flow field. The grid blocks have point and slope continuity at each interface. This simplifies the boundary condition treatment needed at the surface of grid blocks. Freestream boundary conditions are specified on the left side of regions two and three. The grid is body-fitted to the ramp, slot and cowl. While adaptive grids are useful and necessary for some applications[3], frozen grids (at various densities and distributions) are effective for the present application. As shown in Figure 2, the length scales of the grid intervals vary widely over the analysis domain. The smallest grid intervals are generally located in critical regions as follows:

- o boundary layers,
- o free shear layers,
- o rapid compression/expansion regions,
- o shocks, and
- o stagnation regions.

To simplify the notation for grid size definition, grid sizes are defined by a cluster of numbers separated by commas. The numbers between the commas are the interval counts in x by y directions of the grid in region 1, region 2 and region 3, respectively The grid sizes employed are (10x5, 27x17, 22x12), (21x10, 54x34, 44x24), and (42x18, 106x66, 46x26). These three grid sizes are labeled coarse, medium and fine, respectively. The influence of grid on resolution is considered relative to accuracy produced by pairs of grids (coarse/medium, coarse/fine, medium/fine.) Only the coarse and fine grid results are shown.

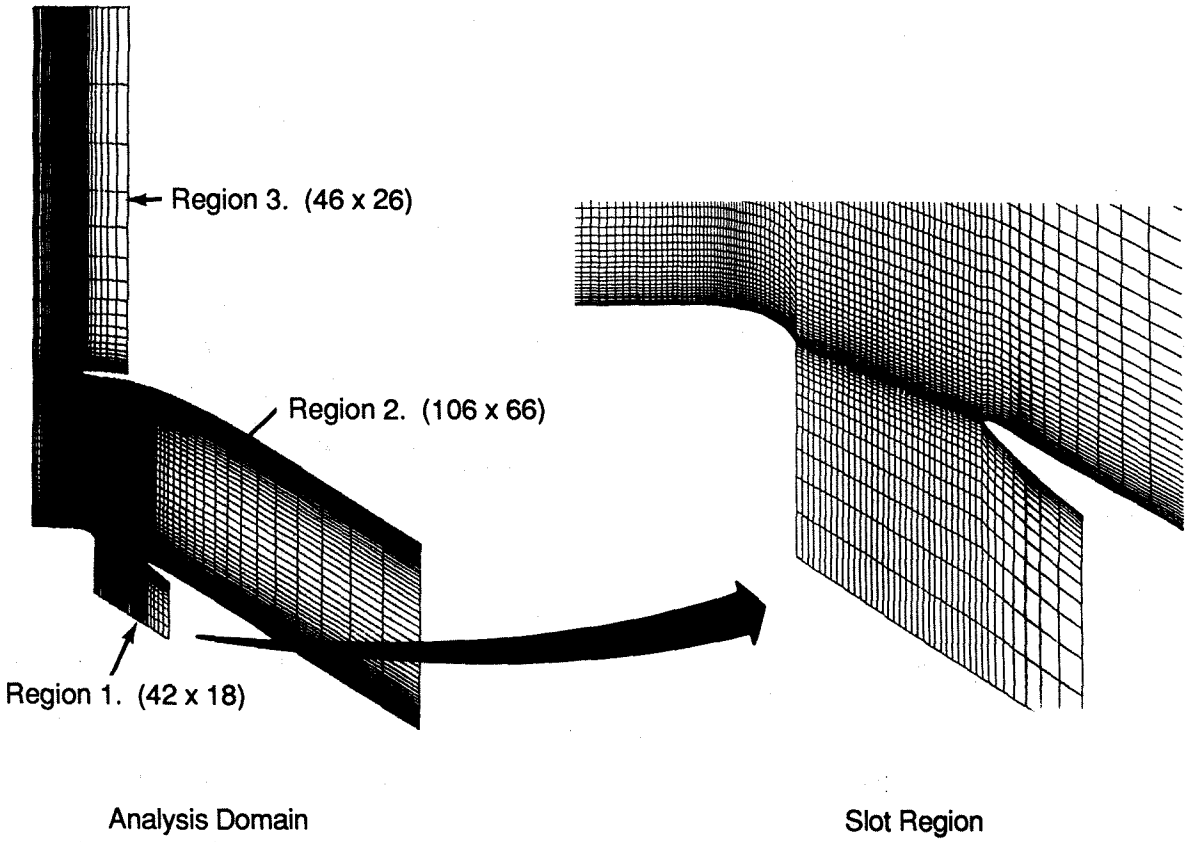

Figure 2. Fine Grid

C. Computational Results

There are many parameters to study in attempting to form an understanding of promising error norm guides for choosing residual level selection and for directing choices in the selection of the grid needed for flow analysis of desired accuracy. Thus far this paper discussed what are believed to be the most prominent causes and measures of error. Discussion of the behavior of some of these error measures with illustrations are the subjects of this section.

The parameters of interest in the presentation of this section are the total pressure profiles, artificial diffusion ratio contours, and Mach contours. All of these parameters except for the artificial diffusion ratio are traditional parameters for error assessment. Note that the artificial diffusion ratio is shown in conjunction with the Mach contours and does not replace these because physical features simply are not revealed by the artificial diffusion ratio. In fact, the artificial diffusion ratio should be void of physical features except near shocks. Mach contours show physical features including shocks.

Figures 3 through 7 provide a basis to determine the analysis accuracy relative to smoothing coefficient level and to grid refinement selection. Figure 1 shows the traverse station for the total pressure ratio, $P_t/P_{t\infty}$, in the throat region of the inlet. Figure 3 shows the improvement in the total pressure with respect to grid refinement and with respect to reducing the artificial smoothing. Note that the degradation of the total pressure results from excessive smoothing or from too coarse a grid. Also note that the results improve with respect to grid refinement even with abnormally high smoothing coefficients. Ultimately grid refinement is the critical issue. However, the efficiency of using a particular grid is improved by setting smoothing coefficients near the stability limit, rather than to maximize convergence. Further examples of this behavior are now discussed.

Figures 4 through 7 are comparisons of solution results for selected grids and smoothing coefficients. Figures 4 and 5 show the effect of smoothing level on ADR for coarse, and fine grids, respectively. Figures 6, 7, and 8 are Mach number contours. Figures 4 and 5, and Figures 6 and 7 show the effect of grid density. Comparison of Figures 4 and 5 with Figures 6 and 7 show that ADR rises sharply with increased smoothing levels and with increased grid coarseness. Note that when ADR is above 0.01 (except for shocks where ADR should be about 0.01), too high a smoothing level or too coarse a grid is indicated. In these regions, the grid must be refined or the smoothing level must be reduced.

It is possible to generate a composite effect of all of these error sources on a particular grid. The grid used for this purpose is shown in Figure 2. Figure 8 shows an example of Mach number contours for the aperture region. Note the agreement between the shadowgraph of the flow field for an experimental test of this inlet and the predicted result for the same flow field (Figure 8).

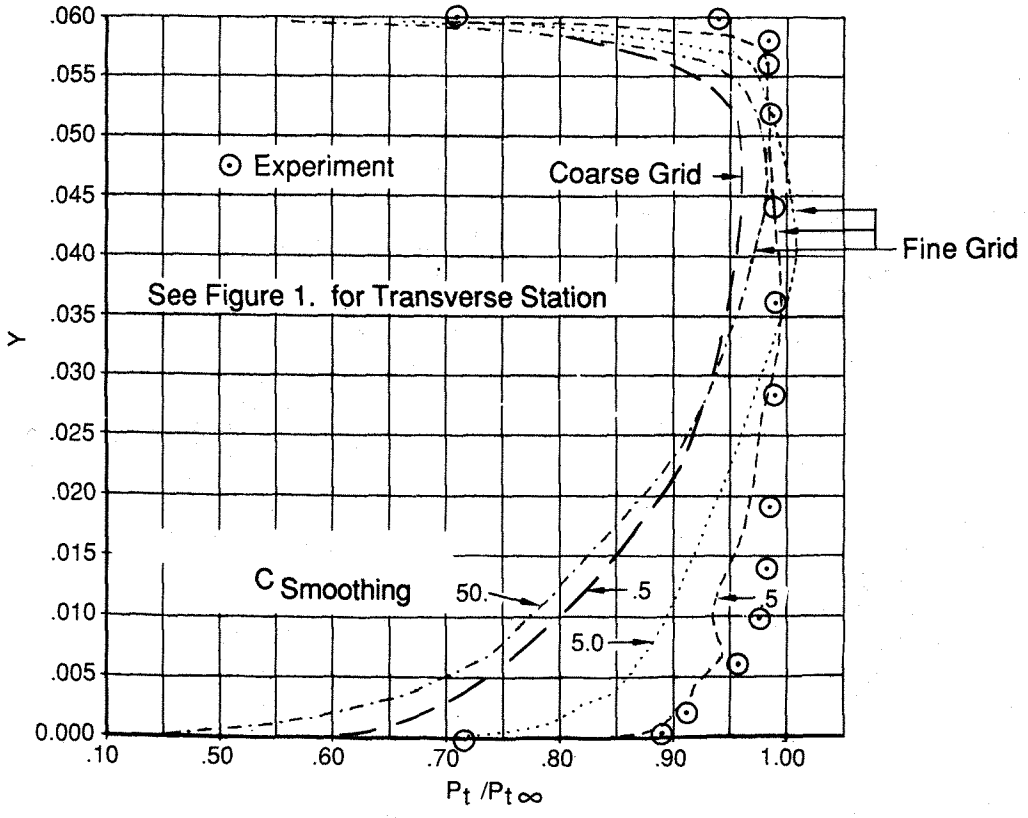

Figure 3. Total Pressure Ratio in Throat Region

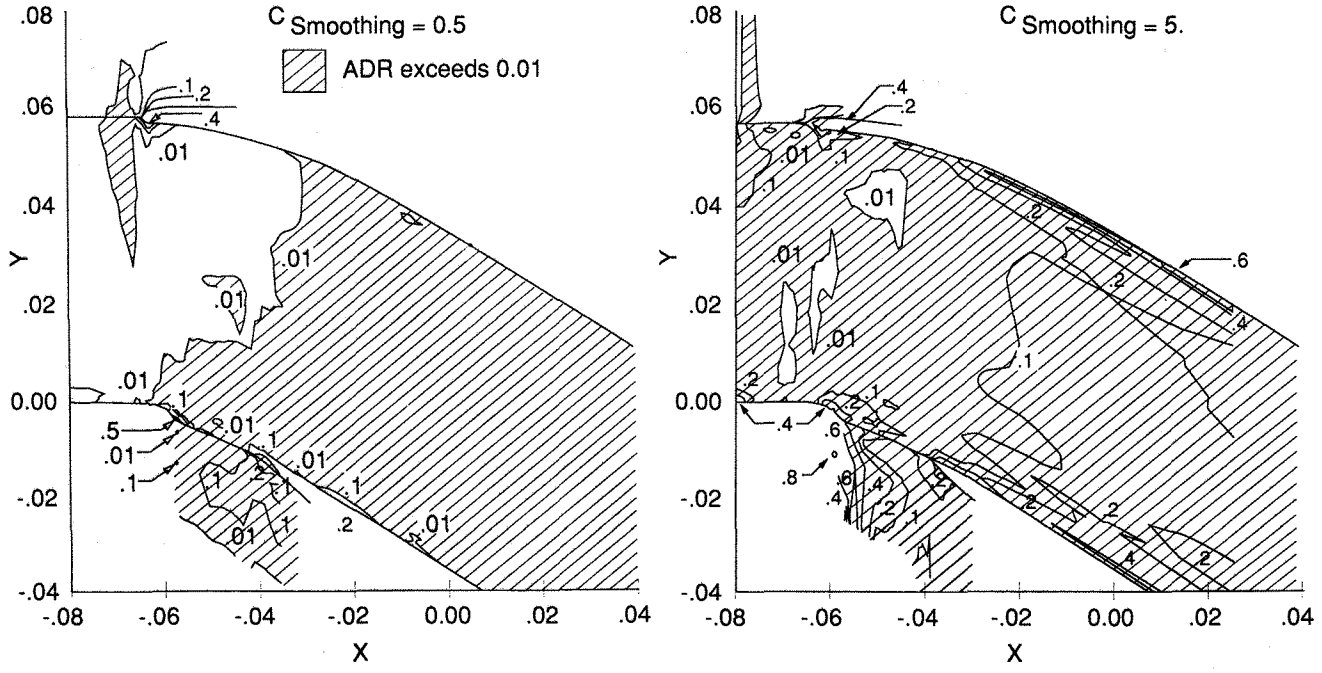

Figure 4. Coarse Grid Artificial Diffusion Ratio Contours

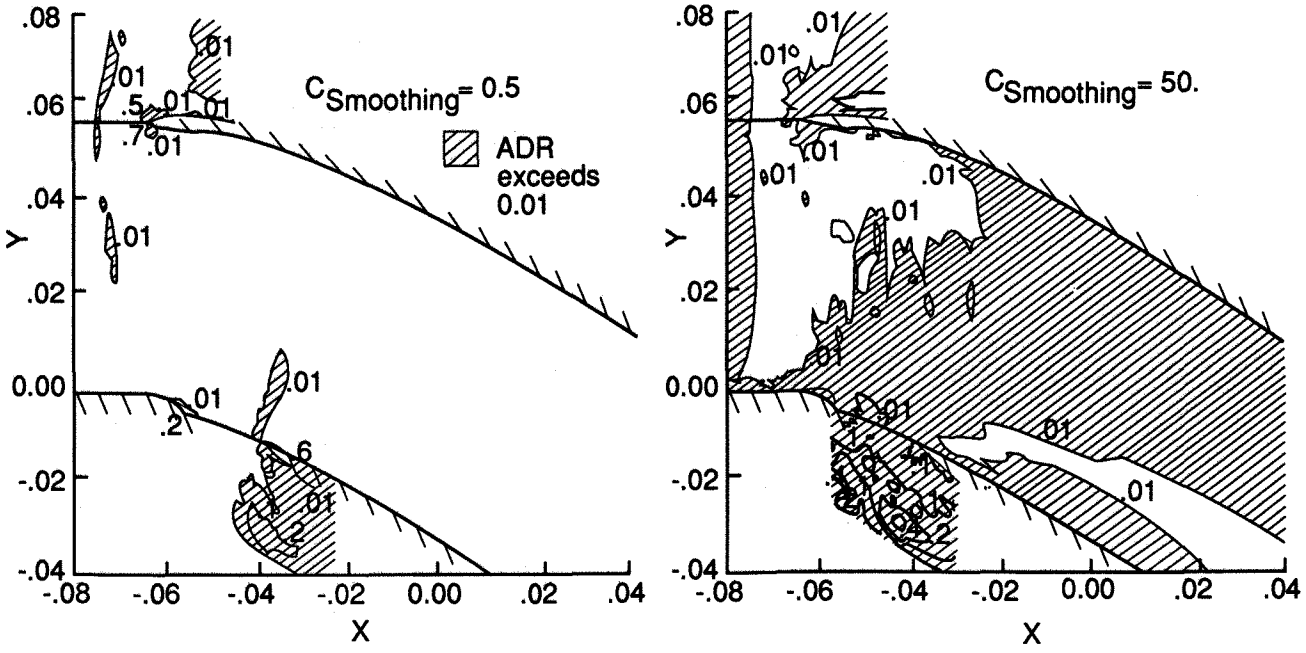

Figure 5. Fine Grid Artificial Diffusion Ratio Contours

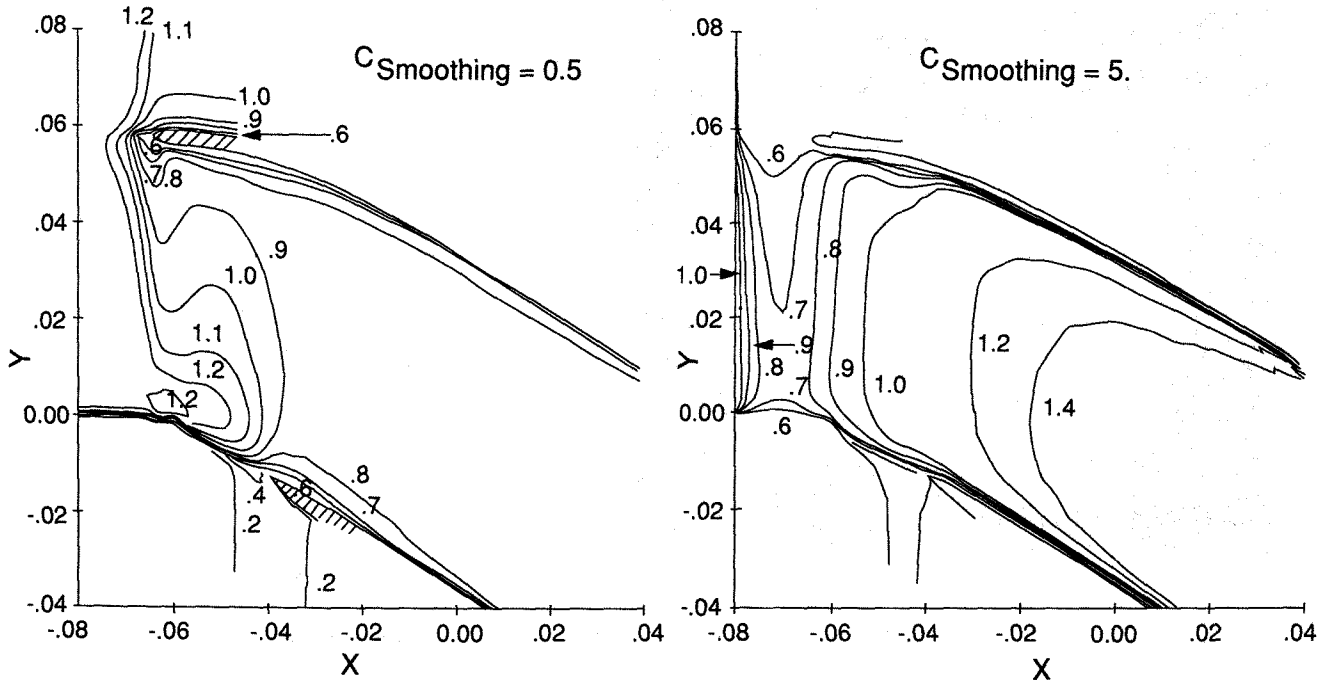

Figure 6. Coarse Grid Mach Contours

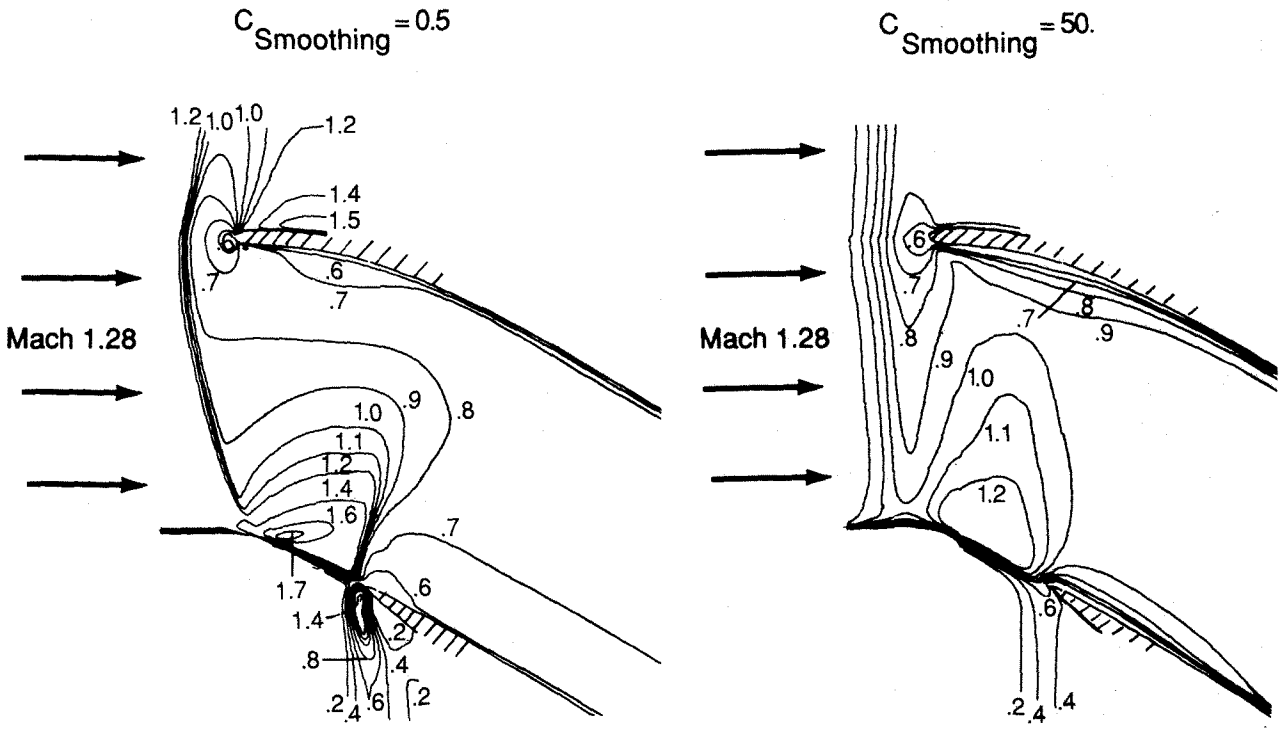

Figure 7. Fine Grid Mach Contour

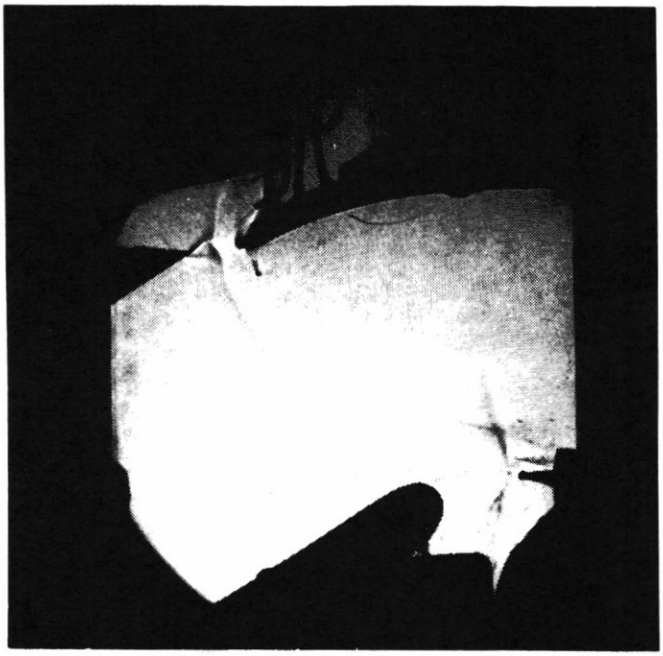

Shadow Graph

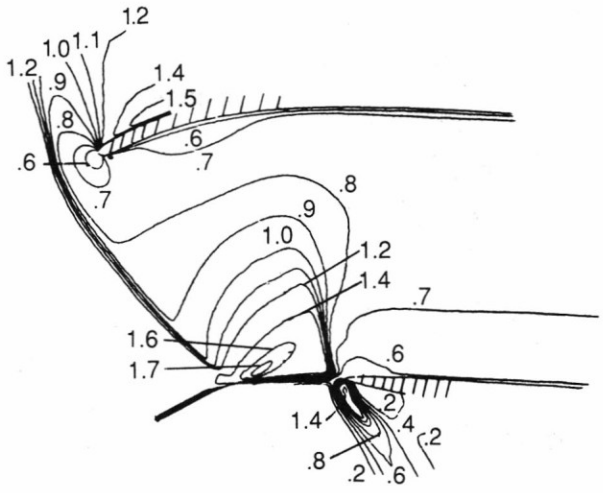

Predicted Mach Contours

Figure 8. Comparison of Experiment with Analysis

V. Conclusions and Recommendations

The solution of the flow field in the aperture region of an external compression inlet with bleed and spillage flow by Navier-Stokes analysis has been presented. A new approach is being developed to streamline and simplify this process. Measures of numerical errors in the analysis process have been explored including, total pressure, and artificial diffusion ratios for mass, energy, and momentum. Preliminary correlation of these error measures show that the artificial diffusion ratio (ADR) provides guidance for grid and smoothing level selection.

The application of ADR leads to a grid choice that yields an adequate solution to the flow field. Comparison of this solution with experiment shows good agreement.

Further work is recommended for demonstrating the utility of ADR on other test problems. These test problems should include comparisons of analysis with benchmark experiments. Further work is recommended for testing the utility of ADR in analysis problems requiring Navier-Stokes computations for the design of aircraft components (both model scale and full scale).

Acknowledgements

The authors are indebted to several people for their valuable assistance and contributions during the preparation of this paper. Dr. Gerald Paynter (Boeing Advanced Systems, Hypersonic Technology Staff) provided advice, guidance, and valuable suggestions for the performance of this study. Mr. Dave Mayer (Boeing Advanced Systems, Propulsion Technology Staff) provided valuable suggestions in the reporting of this work. Special thanks to Dr. James Wilson of the Air Force Office of Scientific Research (AFSC) for funding this work.

References

1. Paynter, G. C. and H. C. Chen, "Progress Toward the Analysis of Supersonic Inlet Flows", AIAA-83-1371, June 1983.

2. Anderson, B. H. "Three-Dimensional Viscous Design Methodology for Advanced Technology Aircraft Supersonic Inlet Systems," NASA TM 83558, January 1984.

3. Peery, K.M. and C.K. Forester, "Numerical Simulation of Multistream Nozzle Flows," AIAA Journal, Vol 18, No. 9, September 1980, pp. 1088-1093.

4. MacCormack, R.W. and B.S. Baldwin, "A Numerical Method for Solving the Navier-Stokes Equation with Application to Shock-Boundary Layer Interactions," AIAA Paper 75-1, January 1975.

5. Forester, C. K., "Error Norm Guided Flow Analysis," Report #1, AFOSR Contract Number F49620-84-C-0037, April 1985.

6. Paynter, G. C., C. K. Forester and E. Tjonneland, "CFD for Engine-Airframe Integration," Journal of Engineering for Gas Turbines and Power, Vol. 109, April 1987.

7. Campbell, A. F. and C. K. Forester, "Evaluation of a Method for Analyzing the Aperture Region of Two-Dimensional External Compression Inlets," AIAA-85-3072, October 1985.

8. Campbell, A. F, J. Syberg, C. K. Forester, "Design Study of an External Compression Inlet Using a Finite Difference Two-Dimensional Navier-Stokes Code," AIAA-84-1275, June 1984.